

Ultra-broadband and compact polarizing beam splitter in silicon photonics

FANG ZHANG,^{1,2} JIAJIU ZHENG,³  YIPENG SONG,^{1,2} WEIXI LIU,⁴
PEIPENG XU,^{1,2,6}  AND ARKA MAJUMDAR^{3,5,7} 

¹Faculty of Electrical Engineering and Computer Science, Ningbo University, Ningbo, 315211, China

²Key Laboratory of Photoelectric Detection Materials and Devices of Zhejiang Province, Ningbo, 315211, China

³Department of Electrical and Computer Engineering, University of Washington, Seattle, WA 98195, USA

⁴Centre for Optical and Electromagnetic Research, State Key Laboratory for Modern Optical Instrumentation, Zhejiang University, Zijingang Campus, Hangzhou 310058, China

⁵Department of Physics, University of Washington, Seattle, WA 98195, USA

⁶xupeipeng@nbu.edu.cn

⁷arka@uw.edu

Abstract: We design and experimentally demonstrate a polarizing beam splitter (PBS) on a silicon-on-insulator (SOI) platform based on an asymmetric directional coupler. The asymmetric directional coupler consists of a regular strip waveguide and a sub-wavelength grating (SWG) waveguide. Engineering the waveguide dispersion via SWG, the phase-matching condition can be satisfied for TM polarization over a broad bandwidth when the waveguide dimensions are optimized. The coupling region of the realized PBS is $\sim 7.2 \mu\text{m}$ long. For the fabricated PBS, the polarization extinction ratio (PER) is 10–45 dB and the insertion loss is 0.3–2.5 dB for TM polarization while the PER is 14–22 dB and the insertion loss is < 0.6 dB for TE polarization when operating in the wavelength range of 1460–1610 nm.

© 2020 Optical Society of America under the terms of the [OSA Open Access Publishing Agreement](#)

1. Introduction

Tremendous progress has been made in silicon photonic components over the last two decades, revealing their potential to create photonic systems with small footprints, low power consumption, high-speed operation, and low-cost packaging [1]. The silicon waveguides provide a very high index contrast between silicon ($n \sim 3.46$) and its cladding, silicon dioxide ($n \sim 1.45$), enabling strong confinement of light with sub-micron cross sections. However, the enhanced index contrast and aspect ratio of silicon waveguides impose a large modal birefringence [2], making the integrated silicon photonic devices polarization dependent. To eliminate the issue, a polarization diversity system consisting of the polarizing beam splitter (PBS) and polarization rotator [3,4] is used for two orthogonal polarizations [5]. Thus, PBS is an essential functional element in the polarization diversity circuit for separating or combining different polarizations. Various structures were proposed to realize integrated PBS, including multimode interference (MMI) devices [6], Mach-Zehnder interferometers (MZIs) [7], topology optimized device [8], and asymmetrical directional couplers (ADC) [9–16].

Among these structures, the ADC-based PBS provides several advantages including small size ($< 20 \mu\text{m}$), low insertion loss (IL < 1 dB), and high polarization extinction ratio (PER, defined as the ratio between the light intensity at two output ports) [17]. The ADC-based PBSs generally consist of a regular strip waveguide and another special waveguide, thus introducing geometrical asymmetry in the coupling region. By optimally choosing the geometrical parameters, the phase-matching condition can be satisfied for the polarization with weak mode confinement. For the other polarization with strong mode confinement, the phase-matching condition is automatically broken due to the significant phase mismatch. Thus, phase-matched polarization

can be coupled to the adjacent waveguide completely with an appropriate coupling length, while the light in the other polarization state propagates through with negligible coupling to the adjacent waveguide. However, the effective indices and the coupling strength are both strongly sensitive to wavelength variation, leading to a limited working bandwidth for ADC-based PBS.

Bent directional couplers have received great interests in achieving high-performance PBS since it features both broadband operation and compact footprint [11,14,18]. This design has also been extended to cascaded triple-bent-waveguide DCs for realizing a compact PBS [14], which extends the bandwidth to 90 nm with PER > 20 dB for TE mode and > 15 dB for TM mode. In Ref. [19], an excellent PBS based on cascaded triple-bent-waveguide DCs was demonstrated with a length of only ~20 μm . This PBS has a PER of > 20 dB over a bandwidth of ~135 nm. In Ref. [16], the bandwidth of the proposed PBS is further improved to ~175 nm with PER > 20 dB and ~120 nm with PER > 25 dB by carefully designing the ADC consisting of a taper-etched waveguide and a slot waveguide. However, a major disadvantage of such structures is the requirement of a two-step fabrication process.

Sub-wavelength grating (SWG) structures, where higher-order diffraction is suppressed due to subwavelength periodicity, provide the flexibility to engineer both index profiles and dispersion properties and have been used in various silicon photonic devices [20–23]. Benefitting from this new degree of freedom, several PBS structures using SWG are proposed [24–28]. In Ref. [24], the PBS based on grating-assisted contra-coupling does not require precise control of the coupling strength and coupling length and has a PER of ~ 12 dB, but the working bandwidth is limited to only 40 nm as the coupling strength is not strong. In Ref. [25], the PBS with SWG structure has been realized by a simple single etch fabrication process. The major disadvantage is that the coupling region is relatively long (> 30 μm) and the bandwidth fails to cover the entire C band. In this paper, we demonstrate an SWG-based PBS with broad optical bandwidth and short (~ 7.2 μm) coupling region. The embedded SWG affects the effective refractive index of the waveguide resulting in the bandwidth broadening. A PER higher than 10 dB is demonstrated over the 1460–1610 nm wavelength range for both TE and TM polarization. We note that, we recently demonstrated a polarization-independent beam splitter using a similar architecture [29], which shows the versatility of this approach.

2. Design and simulation

The PBS is designed for silicon-on-insulator (SOI) platform with 220 nm silicon layer on the top of the SiO₂ box layer. No upper cladding is used. Figure 1(a) shows a schematic of our SWG PBS, which is based on an ADC consisting of a normal silicon strip waveguide and an SWG with corrugations on the inner sidewall. The top view of the coupling section is shown in Fig. 1(b). An S-bend after the coupling region is used to separate and decouple two waveguides. The offsets for the S-bend are $L_x = 6 \mu\text{m}$, and $L_y = 2 \mu\text{m}$, respectively. For the SWG, the period (Λ), the duty cycle (f) and the corrugation width (W_C) are chosen as 240 nm, 0.5 and 130 nm, respectively, taking into account the minimum feature size allowed by the fabrication process. Since TM polarization has a much stronger evanescent coupling than TE polarization for 500-nm-width waveguide, we satisfy the phase-matching condition for TM polarization in our design to minimize the length of the coupling region and thus a short PBS is obtained.

Figure 2(a) shows the TM coupling-length dispersion curves with different SWG duty cycle f . The coupling length is given by $L_c = \lambda_0 / 2(n_{\text{TM}0} - n_{\text{TM}1})$, where $n_{\text{TM}0}$ and $n_{\text{TM}1}$ are, respectively, the effective indices of the first order (even) and second order (odd) supermodes for TM polarization in the two-waveguide system, $\lambda_0 = 1550 \text{ nm}$ is the wavelength. Here the mode effective indices are calculated using the finite-element method (FEM, Lumerical MODE Solutions). For the conventional directional coupler ($f = 1$), the coupling length exhibits a variation of $\delta L_c \sim 10 \mu\text{m}$ as wavelength range from 1450 nm to 1650 nm. When the duty cycle is chosen as $f = 0.9$, the dispersion for TM polarization can be quite flattened over the calculated wavelength band.

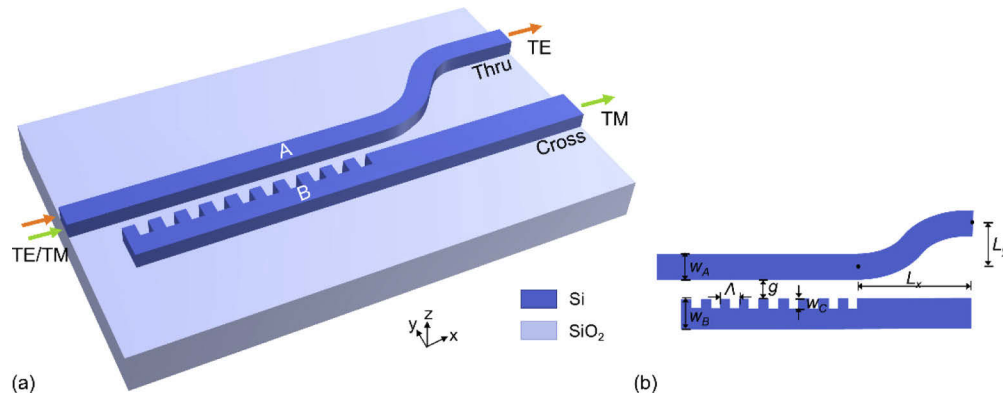


Fig. 1. (a) Schematic of the proposed PBS device; (b) the top view of the coupling section.

However, such a high duty cycle will cause fabrication difficulties. To determine the optimal f , we calculate the TM polarization extinction ratio spectra for the actual device using 3D finite difference time domain (FDTD) method, while the PERs are defined as $10\log_{10}(P_{\text{through}}^{\text{TE}}/P_{\text{cross}}^{\text{TE}})$ and $10\log_{10}(P_{\text{cross}}^{\text{TM}}/P_{\text{through}}^{\text{TM}})$, for TE and TM polarizations respectively. From the spectra shown in Fig. 2(b), when the duty cycle is chosen to be $f=0.5$, the PER is 10–39 dB over a broad wavelength range from 1480 nm to 1650 nm.

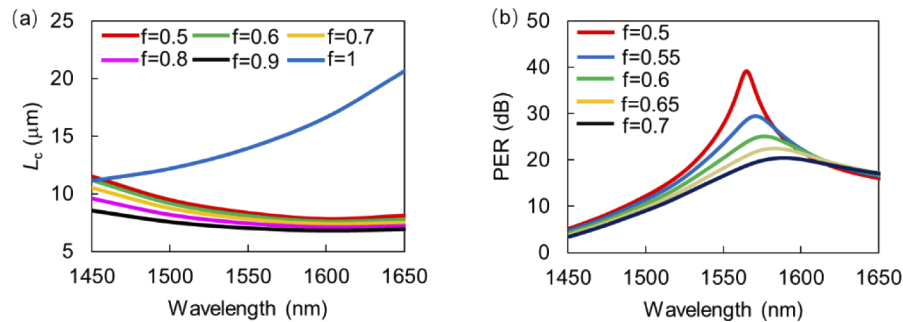


Fig. 2. (a) Calculated TM coupling length dispersion curves with varied SWG duty cycle f ; (b) Calculated TM polarization extinction ratio spectra with varied f .

In order to obtain the optimal width for the SWG waveguide and the length of the coupling region, the light propagation in the full SWG PBS is calculated via 3D FDTD simulation. The mesh in the simulations are set to be $dx = dy = dz = 20$ nm to satisfy the simulation accuracy requirement for the subwavelength structures. The coupling region has a length of $L_c = N \times \Lambda$, where N is the number of SWG periods in the coupling region and Λ is the period. The gap (g) between the two waveguides is chosen to be 200 nm to ensure reliable fabrication of the coupling region. Figure 3 shows the simulated transmission of launched TM input at the wavelength of 1550 nm as the period number N of the SWG in the coupling region varies when choosing different widths for the SWG waveguide ($W_B = 0.555$ μm , 0.56 μm , 0.565 μm , and 0.57 μm). Note that the power to the through port almost becomes zero in the case of $W_B = 0.555$ μm when choosing the period number appropriately ($N = 30$), which indicates that a complete cross coupling from the strip waveguide to the SWG waveguide is happening.

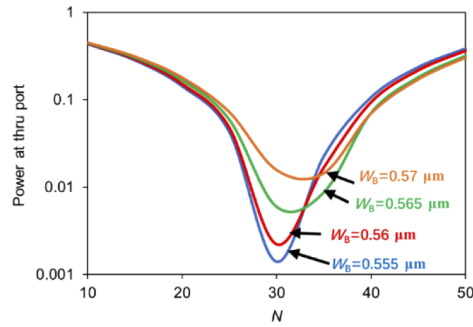


Fig. 3. The simulated transmissions at the through port as the function of the period number N with different width of SWG waveguide ($W_B=0.555\mu\text{m}$, $0.56\mu\text{m}$, $0.565\mu\text{m}$ and $0.57\mu\text{m}$) when the TM mode is launched.

The optimized parameters are summarized as follows: $W_A = 480\text{ nm}$, $W_B = 555\text{ nm}$, $W_C = 130\text{ nm}$, $g = 200\text{ nm}$, $\Lambda = 240\text{ nm}$, $f = 0.5$, $N = 30$ and $Lc = 7.2\text{ }\mu\text{m}$. Figures 4(a) and 4(b) show the simulated light propagation in the designed PBS when the TM and TE modes are launched from the input ports. From the profiles, the input TM light could be evanescently coupled to the cross with negligible residual power at through port, while the input TE light goes directly into the through port without coupling. Figures 4(c) and 4(d) show the calculated spectral response for both polarizations from a wavelength range of 1450 nm to 1650 nm . The ILs are calculated as $10\log_{10}(P_{\text{through}}^{\text{TE}}/P_{\text{input}}^{\text{TE}})$ and $10\log_{10}(P_{\text{cross}}^{\text{TM}}/P_{\text{input}}^{\text{TM}})$, for TE and TM polarizations respectively. We find that the TM mode transmission is wavelength-sensitive, primarily due to the intrinsic wavelength dependence of the evanescent coupling length. Nevertheless, the designed PBS has a bandwidth as broad as 170 nm ($1480\text{--}1650\text{ nm}$) for achieving a PER of $> 10\text{ dB}$. In contrast, the transmission of the TE mode is less wavelength-sensitive. For the TE mode, one has a PER of $> 10\text{ dB}$ and a low loss of $< 0.4\text{ dB}$ over a broad wavelength range from 1450 nm to 1650 nm .

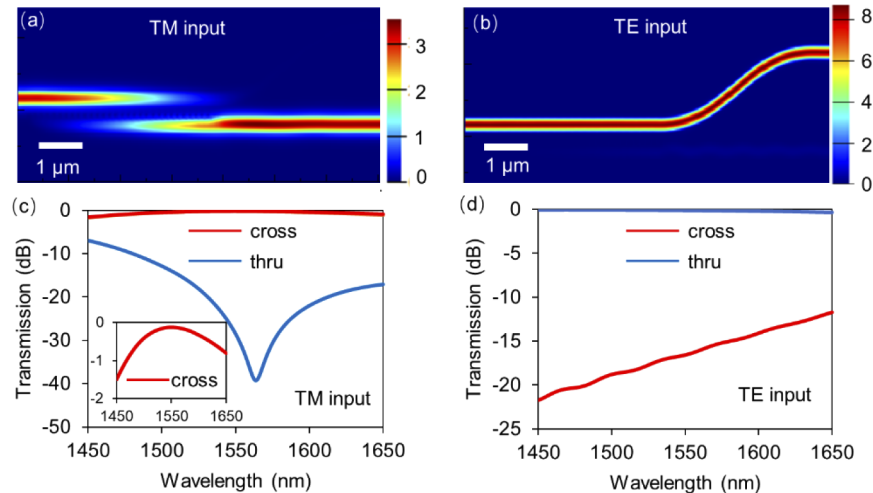


Fig. 4. Simulated light propagation along with the device for (a) TM polarization and (b) TE polarization, and transmission at through and cross port for (c) TM polarization (Insert: enlarged view of the transmission at the cross port) and (d) TE polarization. Here, $W_A = 480\text{ nm}$, $W_B = 555\text{ nm}$, $W_C = 130\text{ nm}$, $g = 200\text{ nm}$, $\Lambda = 240\text{ nm}$, $f = 0.5$, $N = 30$.

3. Fabrication and measurement

The designed SWG PBSs were then fabricated using SOI wafers with a 220-nm-thick silicon layer on top of a 3- μm -thick buried oxide layer. The pattern was defined by a JEOL JBX-6300FS 100 kV electron-beam lithography (EBL) system using a positive tone ZEP-520A resist and transferred to the silicon layer by inductively coupled plasma (ICP) etcher utilizing a gas mixture of SF_6 and C_4F_8 . To characterize the performance for both TE and TM polarizations, appropriately designed grating couplers (GCs) for TE and TM polarizations were used [30], as shown in Figs. 5(a)–5(b). The reference waveguide is the standard single-mode waveguide with the width of 500 nm which were fabricated to measure responses for the TE- and TM- polarized light inputs. Figures 5(c)–5(d) show the scanning electron micrographs (SEM) of the device and the enlarged view of the coupling region. Figures 5(e) and 5(f) show the fully etched TE-type and TM-type focusing sub-wavelength GCs [30]. We probed the devices using an optical fiber setup. The polarization of the input light was controlled to match the fundamental quasi-TE/TM mode of the waveguide by a manual fiber polarization controller (Thorlabs FPC526). A tunable continuous-wave laser (Santec TSL-510) and a low-noise power meter (Keysight 81634B) were used to measure the transmission of the fabricated devices.

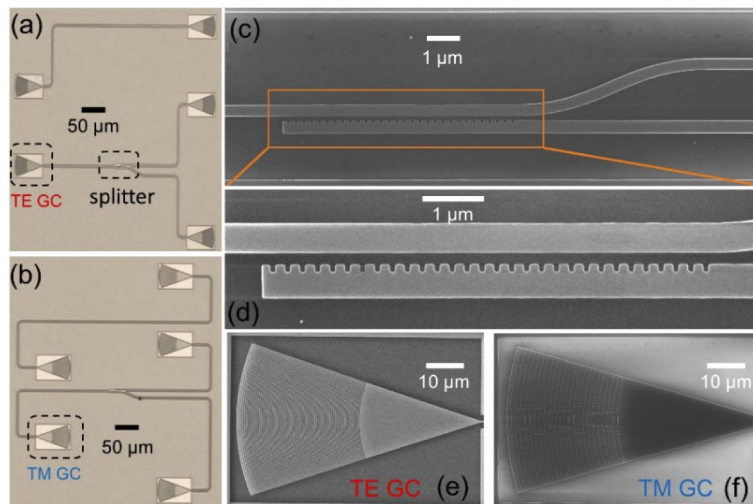


Fig. 5. (a), (b) Optical microscope image of the fabricated SWG PBS. (c), (d) Scanning electron micrograph (SEM) of the device and the enlarged view of the coupling region. (e), (f) SEMs of the GCs.

Figure 6 shows the measured IL and the PER of the fabricated PBS for TE and TM polarizations. The responses are normalized to the transmission of the grating-coupled reference waveguide. The PER at 1550 nm is ~ 18 dB for TE polarization and ~ 45 dB for TM polarization, and the measured ILs are 0.31 dB and 0.84 dB, respectively. For TM polarization, the PER declines when the wavelength is beyond the range 1520 to 1590 nm, which is partly due to the bandwidth limitation of the grating couplers. For the fabricated PBS, the PER ranges between 10–45 dB and the IL is 0.3–2.5 dB for TM polarization while the PER is 14–22 dB and the IL is < 0.6 dB for TE polarization when operating in the wavelength range from 1460 nm to 1610 nm. To check the fabrication tolerance of the present PBS, we also fabricated the devices with different core widths on the same chip, i.e., $W = W + \Delta W$, and $g = g - \Delta W$. In the experiment, we fabricated the PBS with $\Delta W = \pm 20$ nm, and the measured results are shown in Figs. 7(a) and 7(b) for TM- and TE- polarized light. The IL and the PER do not change significantly even when the width is changed up to ± 20 nm: the IL for both polarizations are lower than 1 dB, and the PER remains

higher than 10 dB over a wide bandwidth. Such a good fabrication toleration ± 20 nm is well within the capabilities of current fabrication technologies. Finally, we present a comparison of the silicon-based high-performance experimentally demonstrated PBSs (Table 1), from where we can see that our device shows high performance both in terms of size and bandwidth.

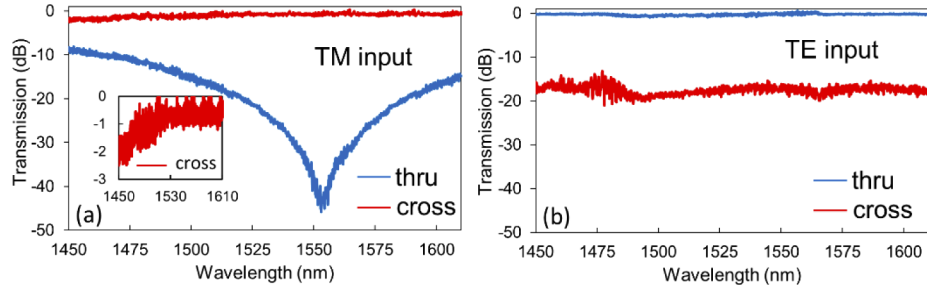


Fig. 6. The measured transmission responses at the cross and through ports for (a) TM polarization (Insert: enlarged view of the transmission at the cross port) and (b) TE polarization.

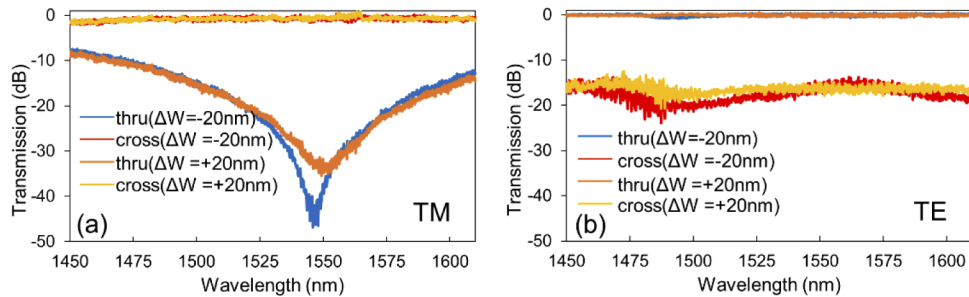


Fig. 7. The measured transmission responses at the cross and through ports for (a) TM polarization and (b) TE polarization of the fabricated PBSs with width variations of $\Delta W = \pm 20$ nm.

Table 1. Performance comparison of several on-chip silicon PBSs.

Ref.	Size (μm)	IL (dB)	PER (dB)	Bandwidth (nm)
Symmetric DC [7]	97.5	0.5	10	>175
Triple straight DC [8]	7.5	2.1	20	90
Bend DC [16]	~ 10	NA	10	<20
Triple Bend DC [12]	26	0.8	20	90
Grating [23]	~ 31.5	1	>20	28
This work	7.2	<2.5	>10	150

4. Summary

In conclusion, we have proposed and experimentally demonstrated a compact and broadband PBS by utilizing an asymmetrical evanescent coupling. The coupling region of the PBS consists of a standard strip waveguide and an SWG waveguide. The coupling length is only $7.2 \mu\text{m}$. The SWG affects the refractive index and their dispersion properties, which is conducive to the bandwidth broadening. Moreover, the PER and IL are 19 dB (40 dB) and 0.31 dB (0.84 dB) for

TE (TM) at the wavelength of 1550 nm. The PER is higher than 10 dB in the wavelength range of 1450–1610 nm for TE polarization and 1460–1610 nm for TM polarization. Besides, the minimum feature size of this device is 120 nm, which can be easily realized by modern fabrication technology. The availability of such broad, compact PBS will find numerous applications in on-chip photonic integrated circuits.

Funding

National Natural Science Foundation of China (61875099, 61505092); Air Force Office of Scientific Research (FA9550-17-C-0017); Natural Science Foundation of Zhejiang Province (LY18F050005); National Science Foundation (0335765, 1337840, 1542101); Zhejiang Province Public Welfare Technology Application Research Project (LGJ18F050001); Ningbo University; National Institutes of Health; Molecular Engineering and Sciences Institute, University of Washington; Clean Energy Institute; Washington Research Foundation; M.J. Murdock Charitable Trust; Altatech; ClassOne Technology; GCE Market; Google.

Disclosures

The authors declare no conflicts of interest.

References

1. L. Chrostowski and M. Hochberg, *Silicon photonics design: from devices to systems* (Cambridge University Press, 2015).
2. D. Dai, L. Liu, S. Gao, D. X. Xu, and S. He, "Polarization management for silicon photonic integrated circuits," *Laser Photonics Rev.* **7**(3), 303–328 (2013).
3. Y. Xiong, J. G. Wangüemert-Pérez, D.-X. Xu, J. H. Schmid, P. Cheben, and W. N. Ye, "Polarization splitter and rotator with subwavelength grating for enhanced fabrication tolerance," *Opt. Lett.* **39**(24), 6931–6934 (2014).
4. M. Ma, A. H. K. Park, Y. Wang, H. Shoman, F. Zhang, N. A. F. Jaeger, and L. Chrostowski, "Sub-wavelength grating-assisted polarization splitter-rotators for silicon-on-insulator platforms," *Opt. Express* **27**(13), 17581–17591 (2019).
5. T. Barwicz, M. R. Watts, M. A. Popović, P. T. Rakich, L. Socci, F. X. Kärtner, E. P. Ippen, and H. I. Smith, "Polarization-transparent microphotonic devices in the strong confinement limit," *Nat. Photonics* **1**(1), 57–60 (2007).
6. J. M. Hong, H. H. Ryu, S. R. Park, J. W. Jeong, S. G. Lee, E.-H. Lee, S.-G. Park, D. Woo, S. Kim, and O. Beom-Hoan, "Design and fabrication of a significantly shortened multimode interference coupler for polarization splitter application," *IEEE Photonics Technol. Lett.* **15**(1), 72–74 (2003).
7. D. Dai, Z. Wang, J. Peters, and J. E. Bowers, "Compact polarization beam splitter using an asymmetrical Mach–Zehnder interferometer based on silicon-on-insulator waveguides," *IEEE Photonics Technol. Lett.* **24**(8), 673–675 (2012).
8. B. Shen, P. Wang, R. Polson, and R. Menon, "An integrated-nanophotonics polarization beamsplitter with $2.4 \times 2.4 \mu\text{m}^2$ footprint," *Nat. Photonics* **9**(6), 378–382 (2015).
9. Z. Lu, Y. Wang, F. Zhang, N. A. F. Jaeger, and L. Chrostowski, "Wideband silicon photonic polarization beamsplitter based on point-symmetric cascaded broadband couplers," *Opt. Express* **23**(23), 29413–29422 (2015).
10. D. W. Kim, M. H. Lee, Y. Kim, and K. H. Kim, "Planar-type polarization beam splitter based on a bridged silicon waveguide coupler," *Opt. Express* **23**(2), 998–1004 (2015).
11. D. Dai, Z. Wang, and J. E. Bowers, "Ultrashort broadband polarization beam splitter based on an asymmetrical directional coupler," *Opt. Lett.* **36**(13), 2590–2592 (2011).
12. X. Guan, H. Wu, Y. Shi, L. Wosinski, and D. Dai, "Ultracompact and broadband polarization beam splitter utilizing the evanescent coupling between a hybrid plasmonic waveguide and a silicon nanowire," *Opt. Lett.* **38**(16), 3005–3008 (2013).
13. D. Dai and J. E. Bowers, "Novel ultra-short and ultra-broadband polarization beam splitter based on a bent directional coupler," *Opt. Express* **19**(19), 18614–18620 (2011).
14. J. R. Ong, T. Y. Ang, E. Sahin, B. Pawlina, G. Chen, D. Tan, S. T. Lim, and C. E. Png, "Broadband silicon polarization beam splitter with a high extinction ratio using a triple-bent-waveguide directional coupler," *Opt. Lett.* **42**(21), 4450–4453 (2017).
15. S. Lin, J. Hu, and K. B. Crozier, "Ultracompact, broadband slot waveguide polarization splitter," *Appl. Phys. Lett.* **98**(15), 151101 (2011).
16. Y. Tian, J. Qiu, C. Liu, S. Tian, Z. Huang, and J. Wu, "Compact polarization beam splitter with a high extinction ratio over S + C + L band," *Opt. Express* **27**(2), 999–1009 (2019).
17. D. Dai, "Advanced Passive Silicon Photonic Devices With Asymmetric Waveguide," *Proc. IEEE* **106**(12), 2117–2143 (2018).

18. J. Wang, D. Liang, Y. Tang, D. Dai, and J. E. Bowers, "Realization of an ultra-short silicon polarization beam splitter with an asymmetrical bent directional coupler," *Opt. Lett.* **38**(1), 4–6 (2013).
19. H. Wu, Y. Tan, and D. Dai, "Ultra-broadband high-performance polarizing beam splitter on silicon," *Opt. Express* **25**(6), 6069–6075 (2017).
20. P. J. Bock, P. Cheben, J. H. Schmid, J. Lapointe, A. Del age, S. Janz, G. C. Aers, D.-X. Xu, A. Densmore, and T. J. Hall, "Subwavelength grating periodic structures in silicon-on-insulator: a new type of microphotonic waveguide," *Opt. Express* **18**(19), 20251–20262 (2010).
21. R. Halir, P. J. Bock, P. Cheben, A. Ortega-Mo ux, C. Alonso-Ramos, J. H. Schmid, J. Lapointe, D.-X. Xu, J. G. Wang emert-P rez,   Molina-Fern andez, and S. Janz, "Waveguide sub-wavelength structures: a review of principles and applications," *Laser Photonics Rev.* **9**(1), 25–49 (2015).
22. P. Cheben, R. Halir, J. H. Schmid, H. A. Atwater, and D. R. Smith, "Subwavelength integrated photonics," *Nature* **560**(7720), 565–572 (2018).
23. R. Halir, A. Ortega-Monux, D. Benedikovic, G. Z. Mashanovich, J. G. Wanguemert-Perez, J. H. Schmid, I. Molina-Fernandez, and P. Cheben, "Subwavelength-Grating Metamaterial Structures for Silicon Photonic Devices," *Proc. IEEE* **106**(12), 2144–2157 (2018).
24. H. Qiu, Y. Su, P. Yu, T. Hu, J. Yang, and X. Jiang, "Compact polarization splitter based on silicon grating-assisted couplers," *Opt. Lett.* **40**(9), 1885–1887 (2015).
25. Y. Zhang, Y. He, J. Wu, X. Jiang, R. Liu, C. Qiu, X. Jiang, J. Yang, C. Tremblay, and Y. Su, "High-extinction-ratio silicon polarization beam splitter with tolerance to waveguide width and coupling length variations," *Opt. Express* **24**(6), 6586–6593 (2016).
26. C. Li and D. Dai, "Compact polarization beam splitter for silicon photonic integrated circuits with a 340-nm-thick silicon core layer," *Opt. Lett.* **42**(21), 4243–4246 (2017).
27. A. Herrero-Bermello, J. M. Luque-Gonz alez, A. V. Velasco, A. Ortega-Mo ux, P. Cheben, and R. Halir, "Design of a Broadband Polarization Splitter Based on Anisotropy-Engineered Tilted Subwavelength Gratings," *IEEE Photonics J.* **11**(3), 1–8 (2019).
28. L. Liu, Q. Deng, and Z. Zhou, "Manipulation of beat length and wavelength dependence of a polarization beam splitter using a subwavelength grating," *Opt. Lett.* **41**(21), 5126–5129 (2016).
29. H. Xie, J. Zheng, P. Xu, J. Yao, J. Whitehead, and A. Majumdar, "Ultra-Compact Subwavelength-Grating-Assisted Polarization-Independent Directional Coupler," *IEEE Photonics Technol. Lett.* **31**(18), 1538–1541 (2019).
30. Y. Wang, X. Wang, J. Flueckiger, H. Yun, W. Shi, R. Bojko, N. A. F. Jaeger, and L. Chrostowski, "Focusing sub-wavelength grating couplers with low back reflections for rapid prototyping of silicon photonic circuits," *Opt. Express* **22**(17), 20652–20662 (2014).